Supplementary Information

Unraveling the timescale of the structural photo-response within oriented Metal-Organic Framework films

Sumea Klokic,[a] Denys Naumenko,[a] Benedetta Marmiroli,[a] Francesco Carraro,[b] Mercedes Linares-Moreau,[b] Simone Dal Zilio,[c] Giovanni Birarda,[d] Rupert Kargl,[e] Paolo Falcaro,[b] Heinz Amenitsch*[a]

[a] *Institute of Inorganic Chemistry, Graz University of Technology, 8010 Graz, Austria, Email: heinz.amentisch@tugraz.at*
[b] *Institute of Physical and Theoretical Chemistry, Graz University of Technology 8010 Graz, Austria*
[c] *IOM-CNR, Laboratorio TASC, S.S. 14, 163.5 km, Basovizza, Trieste 34149, Italy*
[d] *Elettra Sincrotrone Trieste – SISSI Bio Beamline, S.S. 14, 163.5 km, Basovizza, Trieste 34149, Italy*
[e] *Institute of Chemistry and Technology of Bio-Based Systems, Graz University of Technology, 8010 Graz, Austria*

Table of contents

1. Experimental

Materials and methods

All chemicals and solvents are available commercially and were used as received without any further purification. Experiments were performed at ambient pressure and the products are stable at ambient conditions.

Preparation of DMOF-1-on-Cu_2BDC_2-on-$Cu(OH)_2$ films

Copper hydroxide nanobelts were synthesized following the standard protocol described in ref. [1a] and were deposited on sodalime glass substrates following the automated deposition procedure.[2] Prior deposition, the glass substrates (Roth Karlsruhe microscope slides, 1.5 cm x 1.5 cm x 1 mm) were pre-cleaned with distilled water and absolute ethanol. The nanobelt films were fabricated according to the automated nanobelt deposition method,[2] then washed by ethanol and dried in a nitrogen stream prior to their conversion to Cu_2BDC_2, which was performed by immersing the films in a saturated 10 mL terephthalic acid ligand solution (0.65 g in 21 mL dist. water and 56 mL ethanol) at room temperature for 10 minutes. The converted films were washed by ethanol and dried as before. The films were subsequently immersed in 10 mL of an ethanolic zinc acetate solution (25.1 mg Zinc acetate dihydrate in 100 mL ethanol) for two hours, washed gently by ethanol and dried. Conversion to the **DMOF-1**[7] film was subsequently accomplished at 60 °C (heating oven) by tightly sealing the film in a vial containing 10 mL of a methanolic terephthalic acid (7.2 mg) and DABCO (4.8 mg; 1,4-diazabicyclo[2.2.2]octan) solution for 90 min (Figure 1 (a)). The converted film was left to cool to room temperature prior to washing with ethanol and drying. The samples were kept under environmental conditions prior and upon infiltration with azobenzene.

$CuOH_2$: **ATR** ν = 3613, 3305 cm^{-1} (O-H stretch), 930 cm^{-1} (C-O stretch)

DMOF-1: **ATR** ν = 746 cm^{-1}, 1060 cm^{-1} (N-C-H), 1393 cm^{-1}, 1630 cm^{-1} (C=O, C-O stretching modes), 687 cm^{-1} (*trans*-azobenzene), 697 cm^{-1} (*cis*-azobenzene)

Azobenzene: **UV-Vis** (acetone, 25°C): $\lambda_{trans\text{-}azobenzene}$ = 340 nm (ε = 9 939 M^{-1} cm^{-1})

Grazing Incidence Small Angle X-Ray Scattering (GIWAXS) Experiments

GIWAXS measurements on the photo-switching of the grown **DMOF-1** structures as well as measurements prior and upon infiltration by azobenzene were performed at the Austrian SAXS beamline at ELETTRA, Trieste, Italy.[3] An X-Ray beam with a wavelength of 1.54 Å (beam energy 8 keV) was used with a sample to detector distance of 515 mm providing a *q*-range from 0.08 < *q* < 17 nm^{-1}, where *q* denotes the length of the scattering vector ($q = \frac{4\pi}{\lambda}\sin\left(\frac{2\theta}{2}\right)$, λ being the wavelength and θ the scattering angle). The beam size was 0.1 x 0.4 mm (v x h). The angular scale of the detector was calibrated with silver behenate. The samples were mount on a motorized stage with a resolution of 0.001°. Incident grazing angles were in the range 0.2 – 0.3°. For static measurements of the pristine **DMOF-1** thin film prior and after azobenzene infiltration, the 2D GIWAXS patterns were acquired for 60 sec. During the photoexcitation experiments the patterns were acquired for 0.99 s due to the fast kinetics of the structural transformations. A Pilatus3 1M detector was used (Dectris Ltd, Baden Switzerland with active area 169 x 179 mm^2 and a pixel size of 172 µm) and the detector images were processed using SAXSDOG, a software developed at the Austrian SAXS beamline for automatic data reduction.[4] For data analysis, the diffraction patterns of the vertical cut q_V in the out-of-plane direction, the horizontal cut q_H in the in-plane direction as well as radial integration were considered (Figure S1, a). The full 2D pattern radial integration was performed for time-resolved measurements for a better signal to noise ratio. The integrated data were processed with IGOR pro (Wavemetrics, Inc., Lake Oswego, OR). Crystalline phases were associated by using the software GSAS-II[5] and by indexing the relative positions of the Bragg peaks from the scattering patterns. To study the photo-switching behavior of the guest-host system with time-resolved GIWAXS, data were recorded prior to the initiation of the azobenzene isomerization with UV light and throughout the entire subsequent host adaptation until no significant changes in the structure were observed for at least one minute.

Photo-excitation experiments

In this study we employ the flexible **DMOF-1** structure[6] to study the structural transitions when infiltrated with azobenzene.[7] We chose the heteroepitaxial growth of **DMOF-1** starting from the Cu_2BDC_2-on-$Cu(OH)_2$ structure as this approach provides a controlled growth[1a,8] of the **DMOF-1** that allows to limit the film thickness. Photo-switching experiments were performed in combination with time-resolved GIWAXS measurements utilizing the optical on-line table installed at the Austrian SAXS beamline.[9] The sample is positioned on the sample holder, whilst the laser beam is transferred from the optical hutch to the sample position by a specifically designed assembly of motorized optical mirrors and lenses to adjust the incident angle and thus the irradiation spot. The light source to initiate the photo-switch was delivered by the femtosecond laser (Yb:KGW) operating with the third harmonic at 343 nm (250 fs pulse width). We employ a femtosecond laser source to precisely control the photon-flux and thus the photo-response of **DMOF-1/AB**.[9] The laser power was chosen with 8090 mW (RA 25 A) to switch the **DMOF-1/AB** films with a power density of 94.8 mW cm^{-2}. The laser spot size was set with 3.5 mm (FWHM). For the reconversion of the system a blue LED diode operating at 450 nm (PL450B, OSRAM Opto Semiconductors) was installed inside the optical table. The diode power density was set at 17.2 mW cm^{-2} throughout the photo-switching experiments. The spatial overlap between the diode and the UV laser spot on the sample plane was established. Cycling experiments during the photo-switch were performed by remote control of both laser sources. At t = 0 s, the shutter of the 343 nm laser source was opened until no changes in the integrated intensity of the (001) reflection from the **DMOF-1** structure was recorded, then the 450 nm light source was opened for continuous irradiation by closing the UV shutter.

Characterization

X-Ray diffraction measurements were performed using CuKα radiation (λ = 0.154 nm) with the out-of-plane, in-plane and azimuthal angle dependence of the intensity profiles (φ scan) shown in the Supplementary Figure S1 (b) (Rigaku diffractometer, SmartLab, Japan).

Absorbance measurements for the **DMOF-1** thin films prior and after azobenzene infiltration were evaluated using a UV-Vis spectrophotometer (Cary 60, Agilent Technologies).

Infrared measurements of the pristine and infiltrated system were acquired at SISSI-Bio offline end station of the SISSI beamline at Elettra Sincrotrone Trieste[10] using an interferometer VERTEX 70 (Bruker Optics, MA,US), equipped with a DTGS detector and a ATR diamond accessory (MIRACLE, Pike Optics). A reference was collected on the clean crystal and then a spectrum of the sample was recorded averaging 128 scans at 10 kHz scanner speed, with a spectral resolution of 2 cm^{-1}. The *ex-situ* photo switched ON and OFF states were characterized by infrared spectroscopy in the spectral range of 400 – 4000 cm^{-1} operating in transmission mode (Alpha-T, Bruker Optics).

Morphologies of samples were observed by a scanning electron microscope (Field Emission Scanning Electron Microscope Gemini Column (FEG) ZEISS SIGMA 300; WD = 7.1 mm; acceleration voltage 3.00 kV).

Quartz crystal microbalance with dissipation (QCM-D) measurements were realized using the Q-Sense Analyzer (Biolin Scientific), which operates at a resonance frequency of approximately 5 MHz. The experiments were conducted in ambient air or in saturated methanol vapor atmosphere with an open module (QOM 401; sensor QSX 301 gold) at 23°C. In brief, 30 µL of methanol were pipetted in droplets on the Teflon surface of the QOM next to the sensors and covered with a lid measuring 32 x 32 x 9 mm^3, leading to a saturated methanol vapor around the sensor. The measurements were conducted by recording the methanol vapor uptake of every MOF layer (Cu_2BDC_2-on-$Cu(OH)_2$ and subsequent growth of **DMOF-1**(-on-Cu_2BDC_2-on-$Cu(OH)_2$). Each coating was repeated at least on three independent sensors. Reference measurements were made with uncoated sensors, and the mass of the MOF layers was determined by comparing the resonance frequencies of uncoated and coated crystals in air. The mass change was calculated according to the Sauerbrey equation, with $\Delta m \sim C \cdot \Delta f$ (C = 17.7 ng cm^{-2} Hz^{-1}).[11a]

2. System design and characterization

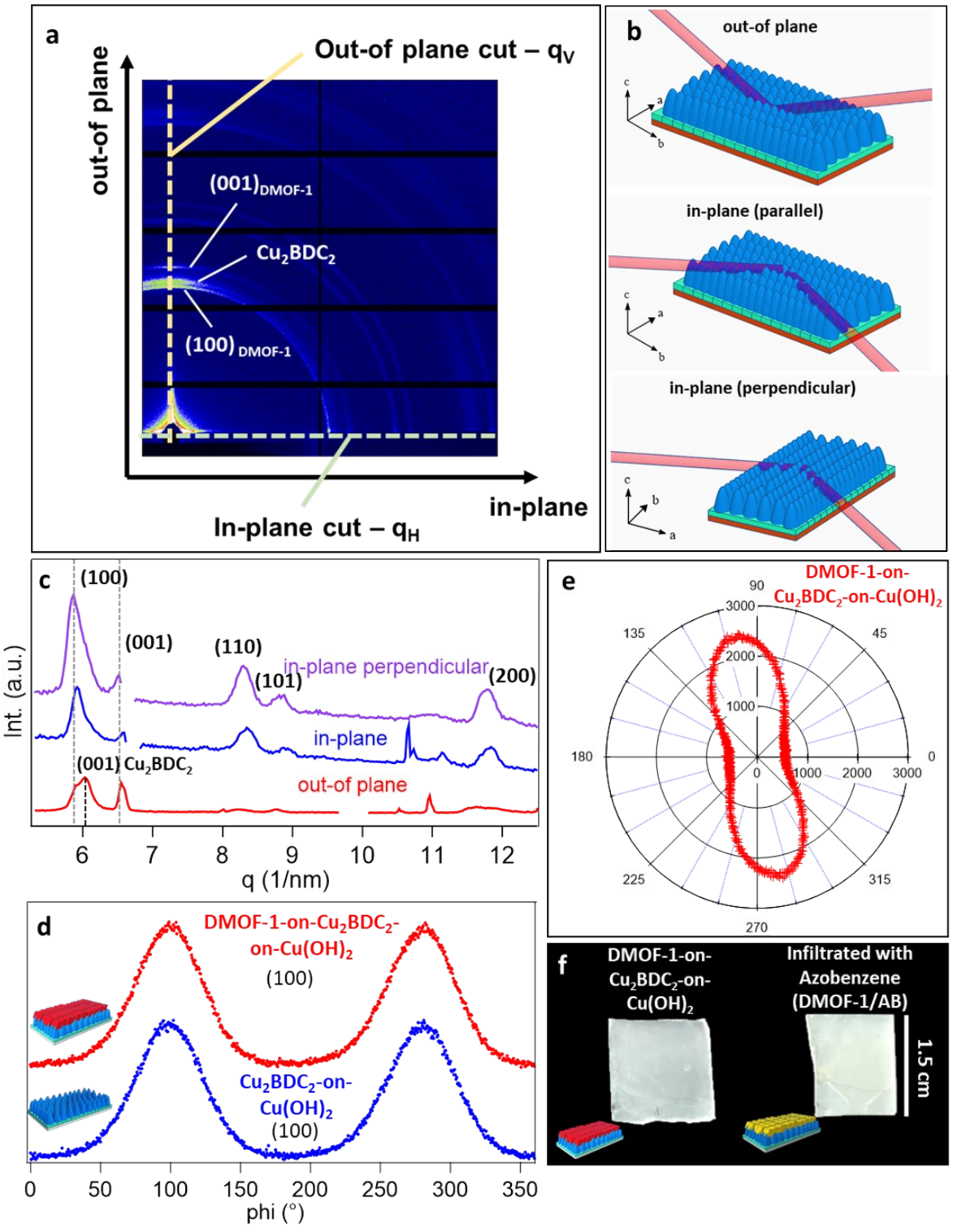

Figure S1 Characterization of DMOF-1 films (glass substrates). a, Integration of 2D detector pattern. Cut margin was selected with 10 pixels for the out-of-plane cut (yellow dotted line) in the q_V range and the in-plane cut (green dotted line) in the q_H range. **b**, XRD measurements. Depicts the different X-Ray beam orientations respective to the **DMOF-1** thin

144 film for the out-of-plane, in-plane parallel and in-plane perpendicular. **c**, Out-of-plane and in-
145 plane GIWAXS patterns of the oriented **DMOF-1** film. **d**, Azimuthal angle dependence of
146 intensity profiles (φ - scan) of the (100) reflection for **DMOF-1** (red line) and the (100) reflection
147 of the Cu_2BDC_2-on-$Cu(OH)_2$ (blue line) with the highest intensity close to 90 and 270°
148 coinciding, indicating that the *a* and *b* axis are oriented in-plane and parallel to the (100)
149 reflection of the Cu_2BDC_2-on-$Cu(OH)_2$. **e**, Polar plot of the (100) **DMOF-1** reflection. **f**, Grown
150 **DMOF-1** film on sodalime glass (an opaque film) and upon infiltration by azobenzene (the film
151 turns yellowish). The film size was usually selected with 1.5 cm x 1.5 cm.

152

3. Degree of orientation evaluation

To perform a quantitative analysis, we examined the intensity distribution of the (100) reflection along the azimuthal angle χ using the GIXSGUI package (Figure S2 (a-b)).[12] The χ-plot shown in Figure S2 (c) allows a simple estimation of the degree of orientation (*DO*)[13] considering the contribution of the isotropic fraction of **DMOF-1/AB** crystallites as highlighted in grey in Figure S2 (d). The *DO* is given by

$$DO\ (\%) = \frac{A_{total} - A_{isotropic}}{A_{total}} \cdot 100$$

where A_{total} is the area below the integrated intensity as a function of χ, and $A_{isotropic}$ is the isotropic fraction as shown in Figure S2 (d). The calculated *DO* was estimated with 45%. This fraction shows that 45% of the **DMOF-1** crystallites have a preferential out-of-plane orientation and is consistent with SEM (Figure S2 (e)).

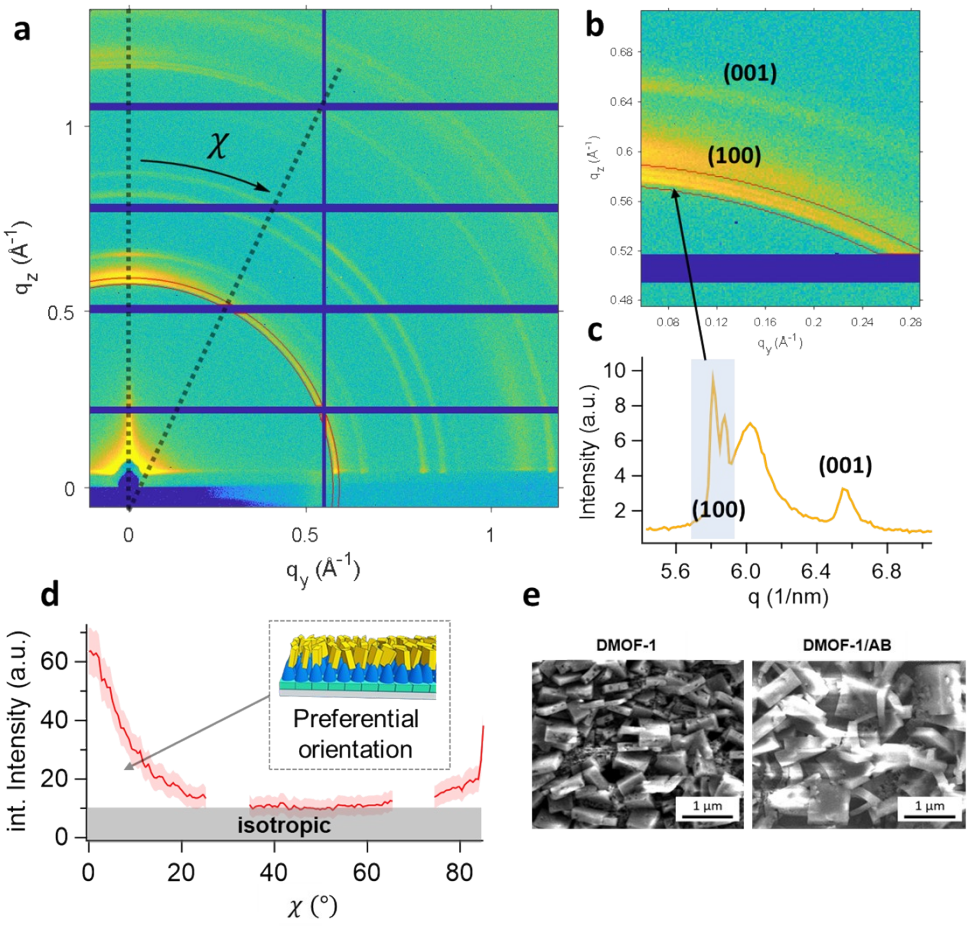

Figure S2 Evaluation of the degree of orientation. a, 2D GIWAXS pattern of the **DMOF-1/AB** film (incident angle 0.3°). The arrow is indicating the direction of azimuthal χ integration

where vertical dashed line is at χ = 0°. **b**, Magnified area of the 2D GIWAXS pattern indicating the intensity distribution of (100) reflections, **c**, together with the corresponding q-range (dark arcs). **d**, Integrated intensity as a function of the azimuthal angle χ of the **DMOF-1/AB** film. The grey area indicates the contribution of the isotropic fraction of **DMOF-1/AB** crystallites, whilst the 0° orientation corresponds to crystallites whose (100) planes are parallel to the substrate (FWHM = 18°),[13] with the crystallites itself growing perpendicular to the substrate (see schematics) that is consistent with the SEM images shown in (**e**). **e**, The **DMOF-1** crystallites retain their morphology after the infiltration by azobenzene into the pores (**DMOF-1/AB**).

4. Quartz crystal microbalance (QCM) measurements

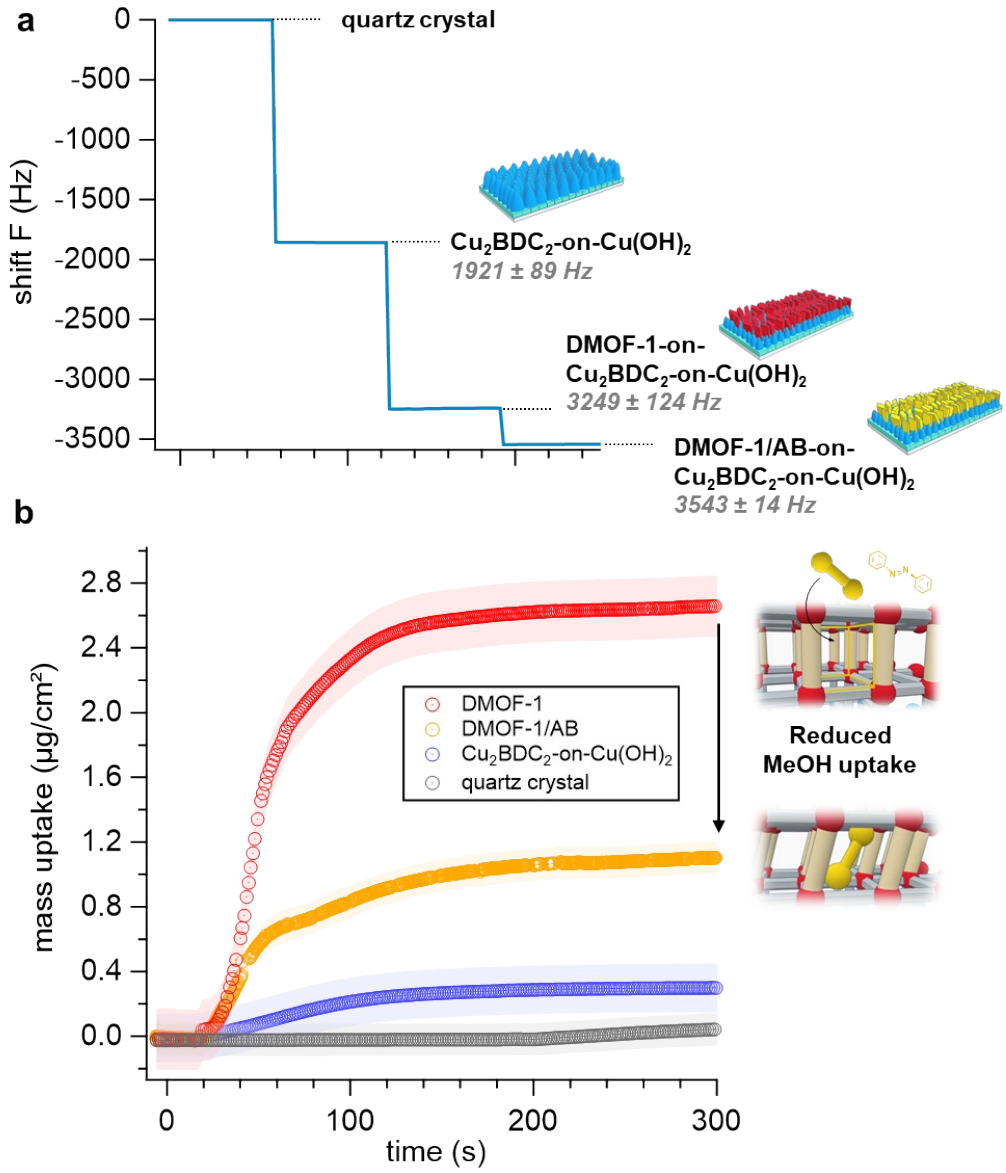

Figure S3 Uptake of methanol by the MOF-on-MOF film system measured by QCM-D. a, Gravimetric measurements of the respective film layers in air (**DMOF-1**-on-Cu_2BDC_2-on-$Cu(OH)_2$) and upon azobenzene infiltration demonstrate the successive increase in the total film mass. **b**, Uptake of methanol vapor by reference quartz crystal (grey trace) is weak compared to the first MOF layer, Cu_2BDC_2-on-$Cu(OH)_2$ (blue trace), which adsorbs 0.2 µg/cm² that is in good agreement to previously reported results.[11b] The subsequent growth of the upper **DMOF-1** film layer (red trace) shows a significantly higher methanol uptake (2.6 µg/cm²) which is owed to the three-dimensional framework structure.[6] Occupying the **DMOF-1** pores by azobenzene (**DMOF-1/AB**) suppresses the methanol uptake. The methanol uptake was

187 reduced by 58% upon azobenzene infiltration within the **DMOF-1** pores. The shaded area
188 corresponds to the 95% confidence interval based on 9 measurements.

5. Azobenzene infiltration process into DMOF-1 films

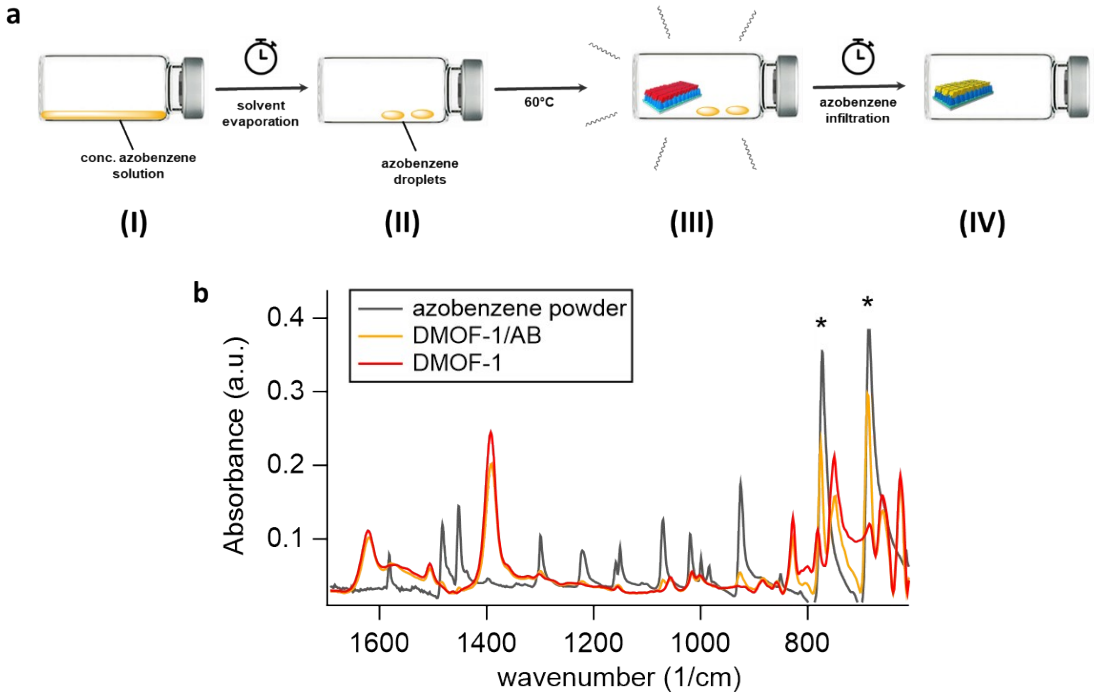

Figure S4 DMOF-1 infiltration by azobenzene. a, Schematic description of the azobenzene infiltration process. In a glass vial, 60 µL of a 10 mg/mL acetonic azobenzene solution is left for the solvent to evaporate (I) and azobenzene droplets are left (II). We use acetone as the solvent to ensure a complete evaporation prior to the MOF-film placement in order to avoid the infiltration of solvent molecules within the MOF pores. The volume is calculated accordingly to provide an excess of azobenzene molecules, thus guaranteeing the infiltration of one azobenzene per **DMOF-1** pore. The **DMOF-1** film is dried prior to the infiltration at 60°C for >15 min to ensure solvent evaporation from the MOF pores, then transferred to the vial containing the azobenzene droplets (III). Infiltration by azobenzene is enhanced at 60°C and is typically left for >30 min (IV). The film is typically freshly infiltrated prior to the photo-switching experiments. **b**, Infrared spectra of azobenzene, **DMOF-1** and **DMOF-1/AB**. Compared to the infrared spectrum of powder azobenzene, infiltration of the molecule within the **DMOF-1** pores leaves only the vibrational bands located at ~700 and 650 cm^{-1} pronounced in intensity that correspond to the C-H vibrations of azobenzene. Other vibrational bands are suppressed upon infiltration which indicates that the azobenzene is accommodated within the **DMOF-1** pores.[7a,c]

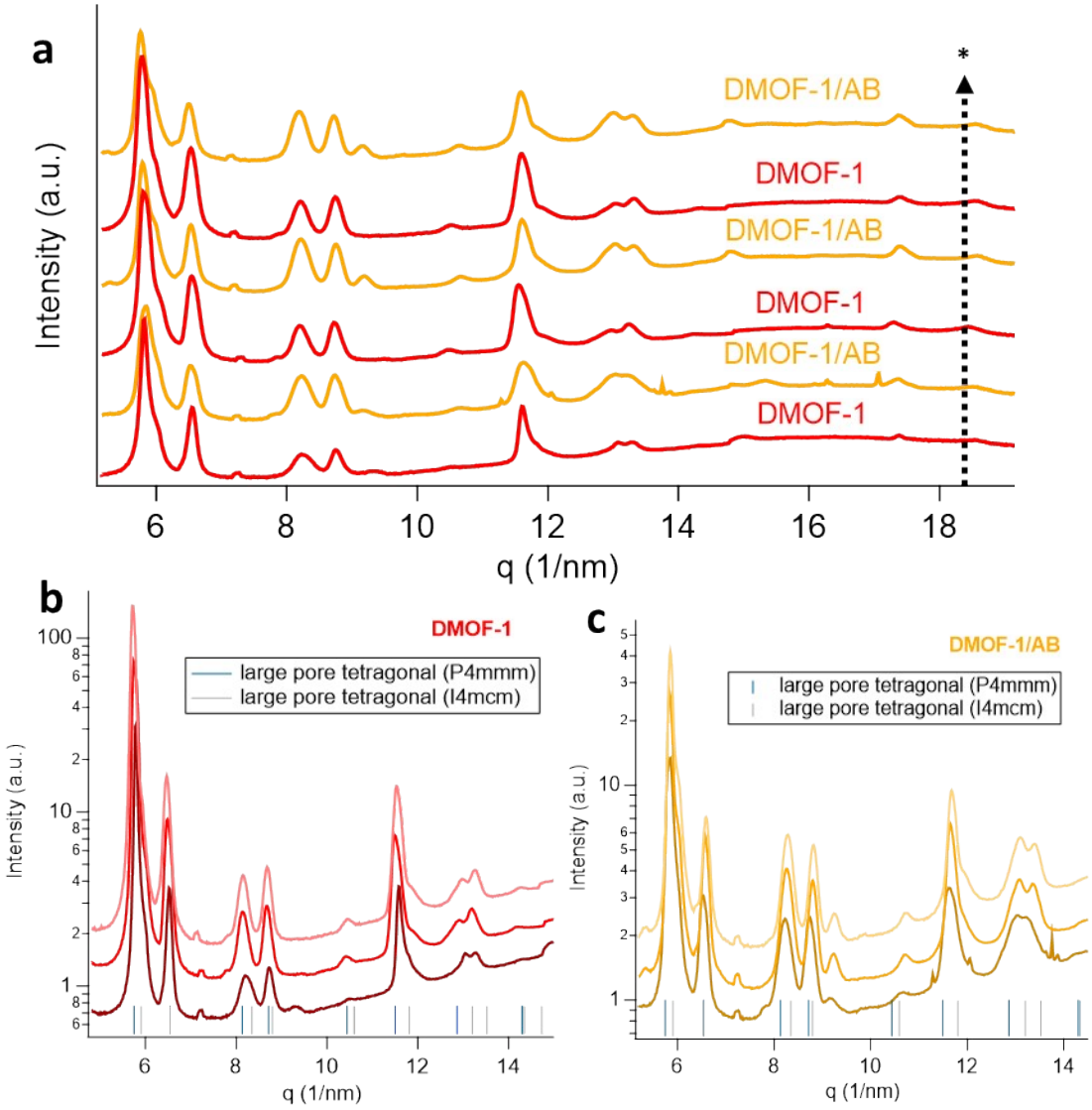

208

209 **Figure S5 Reversible azobenzene infiltration in DMOF-1 films (glass substrates). a,** The
210 prisitine **DMOF-1** thin film (red traces, **b**) was infiltrated as described in Figure S4 yielding the
211 **DMOF-1/AB** guest-host system (yellow traces, **c**). Removal of the chromophore was
212 performed by washing the film with ethanol and drying in N_2 stream. Repeating the infiltration
213 process was found to leave the host system unaltered (arrow indicates the infiltration
214 sequence) as displayed with the inset graphs. **b**, The **DMOF-1** structures were found to match
215 the reported large-pore tetragonal *P4/mmm* space group,[14a] whilst **c**, the infiltrated **DMOF-**
216 **1/AB** system gives a better match with the expected tetragonal narrow pore *I4/mcm* space
217 group.[14a]

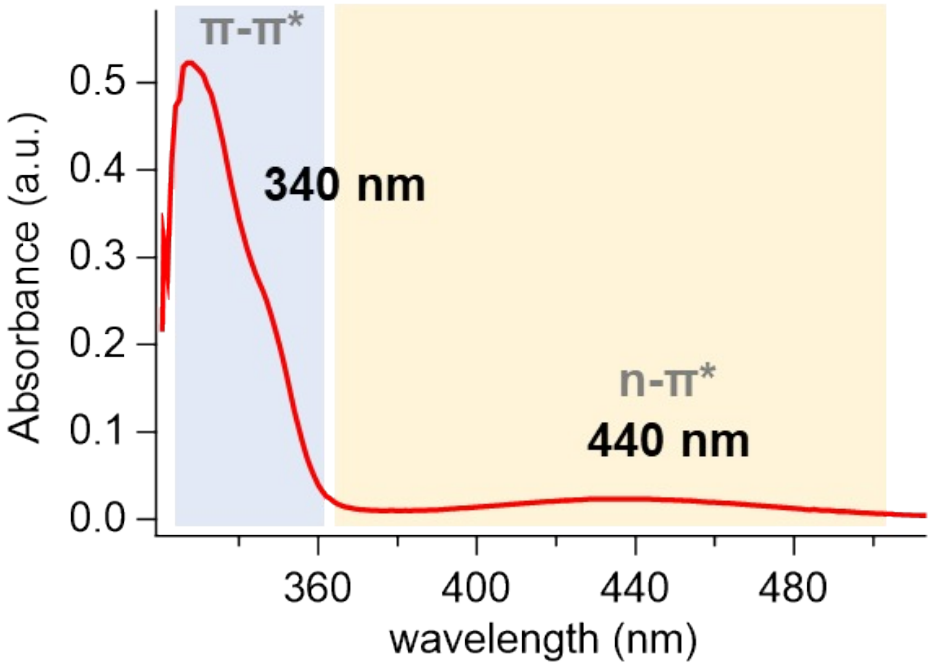

Figure S6 UV-Vis spectrum of an acetonic 0.001 mg mL^{-1} azobenzene solution. The π-π* transition shows the strong absorption band in the ~340 nm range, and the weaker n-π* transition in the range of ~440 nm and is coincident with spectra reported in literature. The sudden drop in intensity <320 nm is owed to the strong absorption of acetone in the UV range.[14b]

6. Polarization angle-dependent absorption measurements at 343 nm

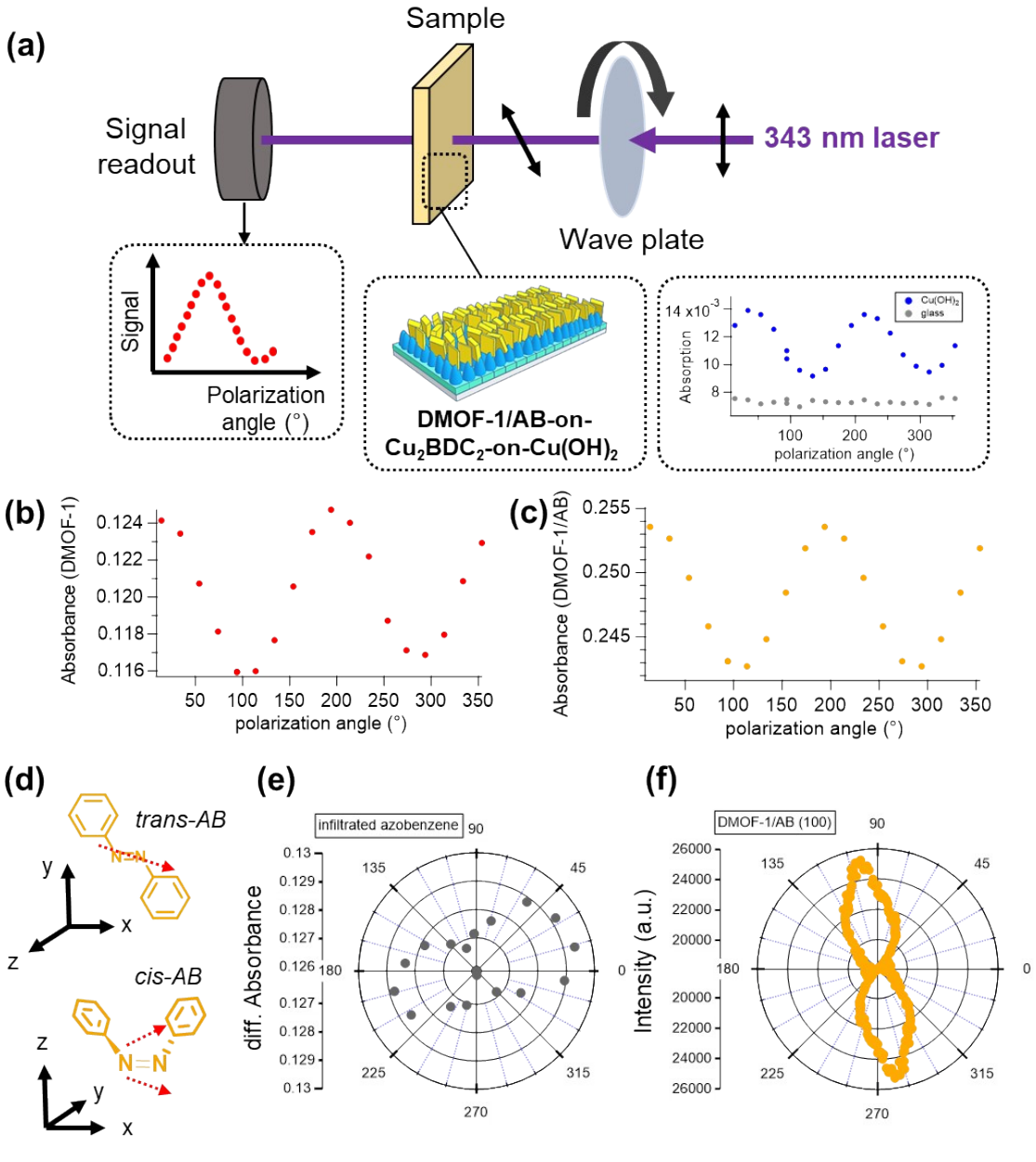

Figure S7 Polarization angle-dependent absorption measurements at 343 nm wavelength. a, The polarization angle dependent absorption of the **DMOF-1/AB** films was measured using 343 nm wavelength laser source and a half-wave plate (Thorlabs) as schematically depicted in the experimental setup. The **DMOF-1/AB** film grown on glass substrates was positioned after the half-wave plate, and the intensity of transmitted light was measured by a UV-sensitive silicon diode (Thorlabs). Reference measurements were performed for bare glass substrates and $Cu(OH)_2$ nanobelts. No polarization dependency was found for the bare glass substrate. **b-c**, Polarization angle dependent measurements of the

DMOF-1 and **DMOF-1/AB** films were found with a strong response, with the absorbance increasing for the azobenzene infiltrated films. **d**, The transition dipole moment of azobenzene is schematically depicted and is approximately along the azobenzene N-N bond in *trans*-configuration.[1b] **e**, Difference (**c**) - (**b**) absorption with the most intense response of the infiltrated azobenzene molecules within the **DMOF-1** pores perpendicular to the (100) reflection of the **DMOF-1/AB** structure **(f)**, testifying a preferential alignment of azobenzene molecules along the *c*-axis direction.[1a] **(f)** Azimuthal angle dependence of intensity profiles (x-ray φ - scan) of the (100) reflection for the **DMOF-1/AB** structure.

7. Time-resolved *in-situ* Grazing Incidence Small Angle X-Ray Scattering

The evaluation of the dynamic switching behavior of the **DMOF-1/AB** films was accomplished by considering the radial integration. This was mainly due to the better statistics provided by the higher number of integrated pixels that consequently provides a better signal-to-noise ratio when compared to out-of-plane integrated data. However, the switching constants remain irrespective on the integration in the range of the mean statistical error obtained in this study.

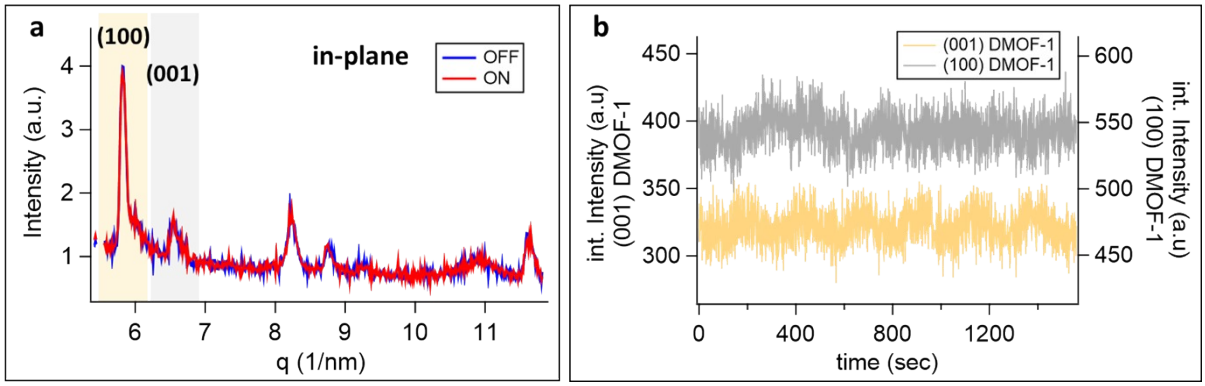

Figure S8 Photo-switching of the DMOF-1/AB structure (glass substrate). a, In-plane integration of the **DMOF-1/AB** structure with the ON and OFF with the ON and OFF photo-response indicated in red and blue, respectively. The structure was photo-cycled reversibly (see Figure S9 b). The yellow and grey areas indicate the range of the integrated intensity for the (001) reflection (*yellow*) and the (001) reflection (*grey*) over the course of the photo-cycling of the structure. **b**, Integrated intensity throughout the photo-cycling for the (100) and (001) reflections shows no structural changes in the in-plane direction due to the rigidly connected **DMOF-1** structure to the Cu_2BDC_2-on-$Cu(OH)_2$.

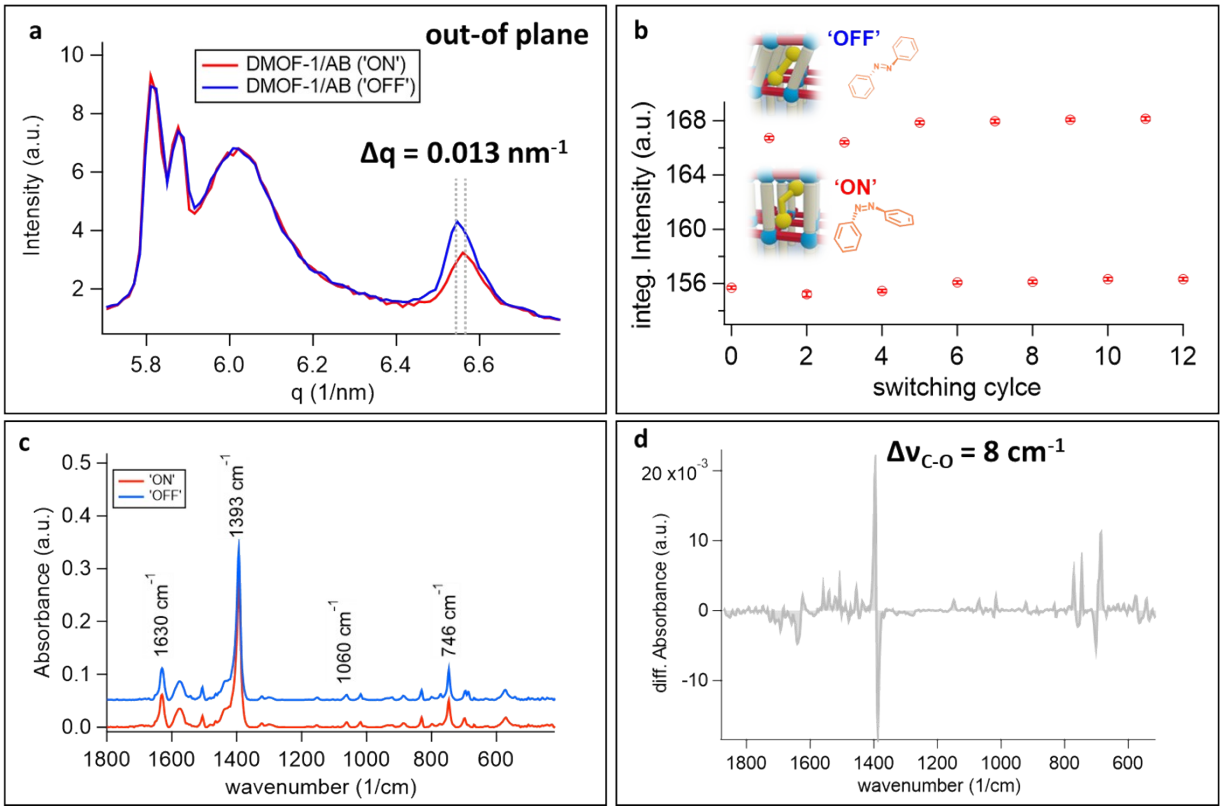

Figure S9 Photo-switching of the DMOF-1/AB structure (glass substrate). a, Out-of-plane integration of the **DMOF-1/AB** structure with the ON and OFF photo-response indicated in red and blue, respectively. Upon photo-switching, the (001) reflection was determined to undergo a shift by Δq = 0.013 nm^{-1} as denoted by the dotted lines. **b**, Photo-switching of **DMOF-1/AB** yields quantitative and fully reversible conversion between the ON and OFF state. The integrated intensity of the (001) reflection for radial integrated data is displayed. **c**, Infrared spectrum of the ON (red trace) and OFF (blue trace). The infrared bands of **DMOF-1/AB** were assigned with 746 cm^{-1} and 1060 cm^{-1} to correspond to the N-C-H vibrations from the pillaring DABCO. The strong band at 1393 cm^{-1} and the weaker band located at 1630 cm^{-1} were attributed to the C-O vibrations arising from the carboxylic groups in the **DMOF-1** framework.[7] **d**, Difference in absorbance between the ON and OFF state show a shift of $\Delta \nu$ = 8 cm^{-1} for the strong C-O vibrational band located at 1393 cm^{-1}.

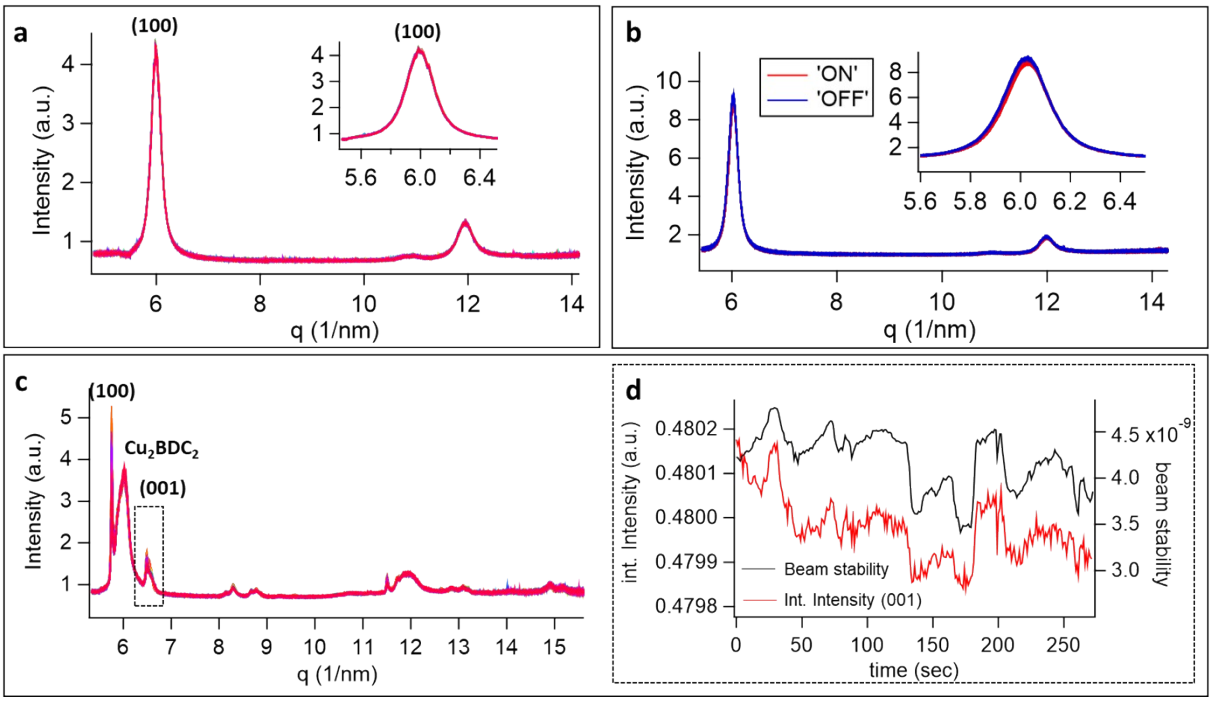

Figure S10 Photoexcitation of Cu_2BDC_2-on-$Cu(OH)_2$ films (sodalime glass substrates). **a**, UV exposure of the as-prepared Cu_2BDC_2-on-$Cu(OH)_2$ film. The inset shows the (100) reflection lacking significant structural changes over the entire exposure period. **b**, Upon infiltration of Cu_2BDC_2-on-$Cu(OH)_2$ by azobenzene and subsequent UV exposure at 343 nm (red trace ON) or to 450 nm (blue trace, OFF) showed no significant changes. **c,** Irradiation of the **DMOF-1**-on-Cu_2BDC_2-on-$Cu(OH)_2$ film system by 343 nm shows no structural changes for the (001) reflection, the variation in the integrated intensity arise solely because of the X-ray beam (**d**).

8. Photo-switching experiments in bulk DMOF-1

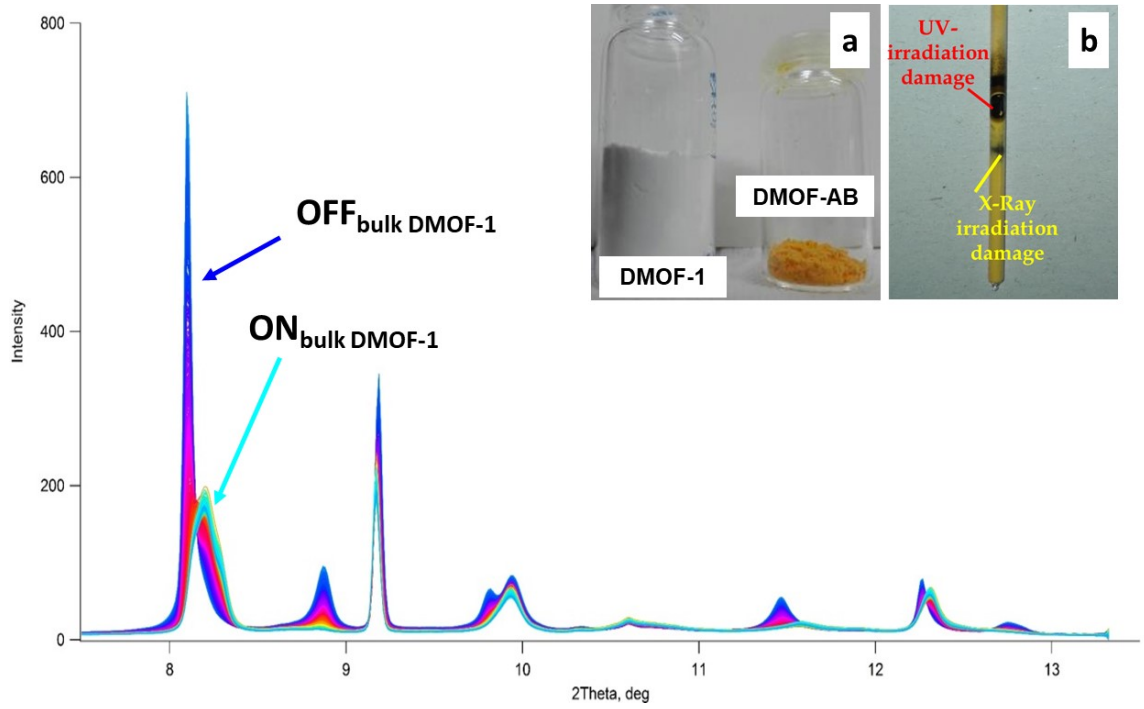

Figure S11 Bulk DMOF-1 photo-switching experiments. **a,** Synthesis of DMOF-1 was slightly modified compared to literature and performed at ambient pressure.[6] In a two-neck flask 2.0 g zinc(II) nitrate hexahydrate was mixed with 1.16 g terephthalic acid and 0.38 g DABCO in 40 mL DMF and stirred at 120°C for 24 hours under refluxing conditions. The colourless precipitate was filtered and dried *in vacuo* prior to infiltration with azobenzene, which was performed according to the procedure reported by Yanai et al.[7] yielding an orange powder. **b**, The infiltrated DMOF-1 bulk powder with azobenzene was exposed to 343 nm UV light (2 W) filled in a quartz capillary (WJM-Glas/Müller GmbH; length = 80 mm, diameter = 1.5 mm, wall thickness = 0.01 mm) for one hour and continuously exposed to synchrotron X-Ray radiation to track ongoing structural changes. Severe irradiation damage was induced due to the low light penetration inside of the capillary.[15] Shorter exposure to UV light was insufficient to induce photo-responsive behaviour. The OFF state (*blue trace*) changed to the ON state (*turquois trace*). These initial photo-switching experiments in bulk revealed that the absorption by the quartz capillary and the low light penetration into the powder have to be out-ruled to achieve high switching conversion and moreover to allow reliable photophysical characterization.[15]

9. IR experiments – photo-isomerization of azobenzene within the DMOF-1/AB film structure

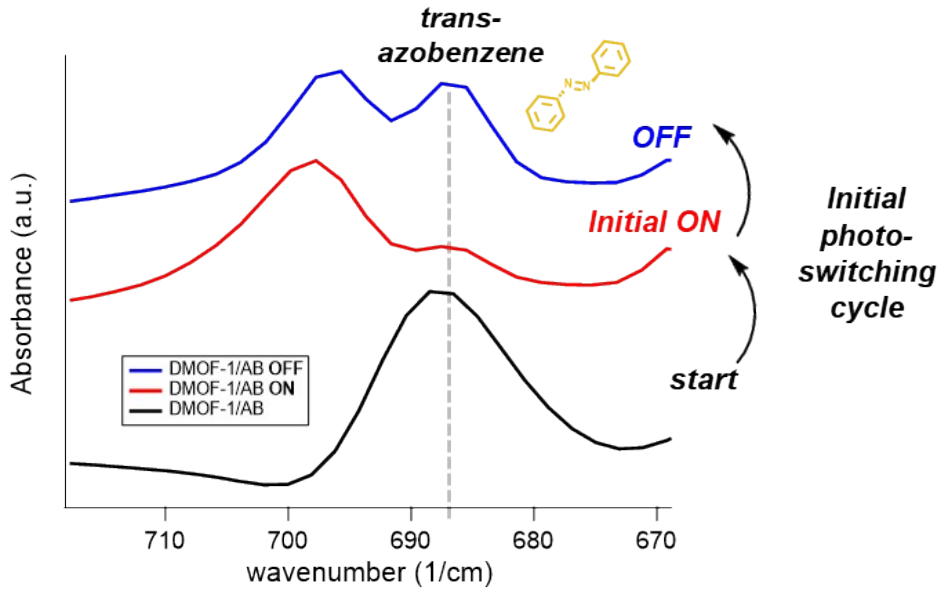

Figure S12 The freshly infiltrated DMOF-1/AB film structure shows a strong vibrational band at 687 cm^{-1} that corresponds to the *trans*-azobenzene (black trace). Initial irradiation by 343 nm of the **DMOF-1/AB** structure (ON state) lead to the *cis*-conformer (red trace). Subsequent irradiation by 450 nm revealed only a partial reconversion to the *trans*-isomer (blue trace).

10. Calculation of the azobenzene loading

To estimate the azobenzene loading per **DMOF-1** pore, calculations according to Koehler *et. al* [16] were performed with the parameters summarized in Table S1.

The azobenzene concentration within the **DMOF-1** pores is calculated by Eq. S1.

$$c_{AB} = \frac{\Delta A}{(\varepsilon_{cis} - \varepsilon_{trans}) * d_{DMOF-1\ film} * \Delta x_{AB}} = 0.79 \qquad \text{Eq. S1}$$

Considering the unit cell volume of the infiltrated **DMOF-1/AB** system[7a] ($V_{DMOF\text{-}1/AB}$ = 2086 Å³) and the Avogadro constant (N_A = 6.6*10^{23}) the loading of azobenzene per unit cell is given by Eq. S2.

$$Loading = c_{AB} * N_A * V_{\frac{DMOF-1}{AB}} = 1.09 \frac{molecules}{unit\ cell} \qquad \text{Eq. S2}$$

This calculation comprises certain uncertainties for all variables[16] and the azobenzene loading serves as an estimate of 1 molecule per **DMOF-1/AB** cell.

Table S1 Parameters for the calculation of the azobenzene loading. ΔA denotes the π-π* band, $\varepsilon_{cis\text{-}AB}$ and $\varepsilon_{trans\text{-}AB}$ the extinction coefficients for the *cis*- and *trans*-isomers. Δx_{AB} refers to the change of the *cis*-content throughout the photo-switch and $d_{DMOF\text{-}1\ film}$ to the thickness of the **DMOF-1/AB** crystallites oriented as the film system.

ΔA (λ = 330nm)	-0.297
$\varepsilon_{cis\text{-}AB}$	2500 L/mol cm[17]
$\varepsilon_{trans\text{-}AB}$	22 000 L/mol cm[18]
Δx_{AB}	0.40
thickness $d_{DMOF\text{-}1\ film}$	0.000048 cm

11. Influence of orientation on the photo-switching of DMOF-1/AB films

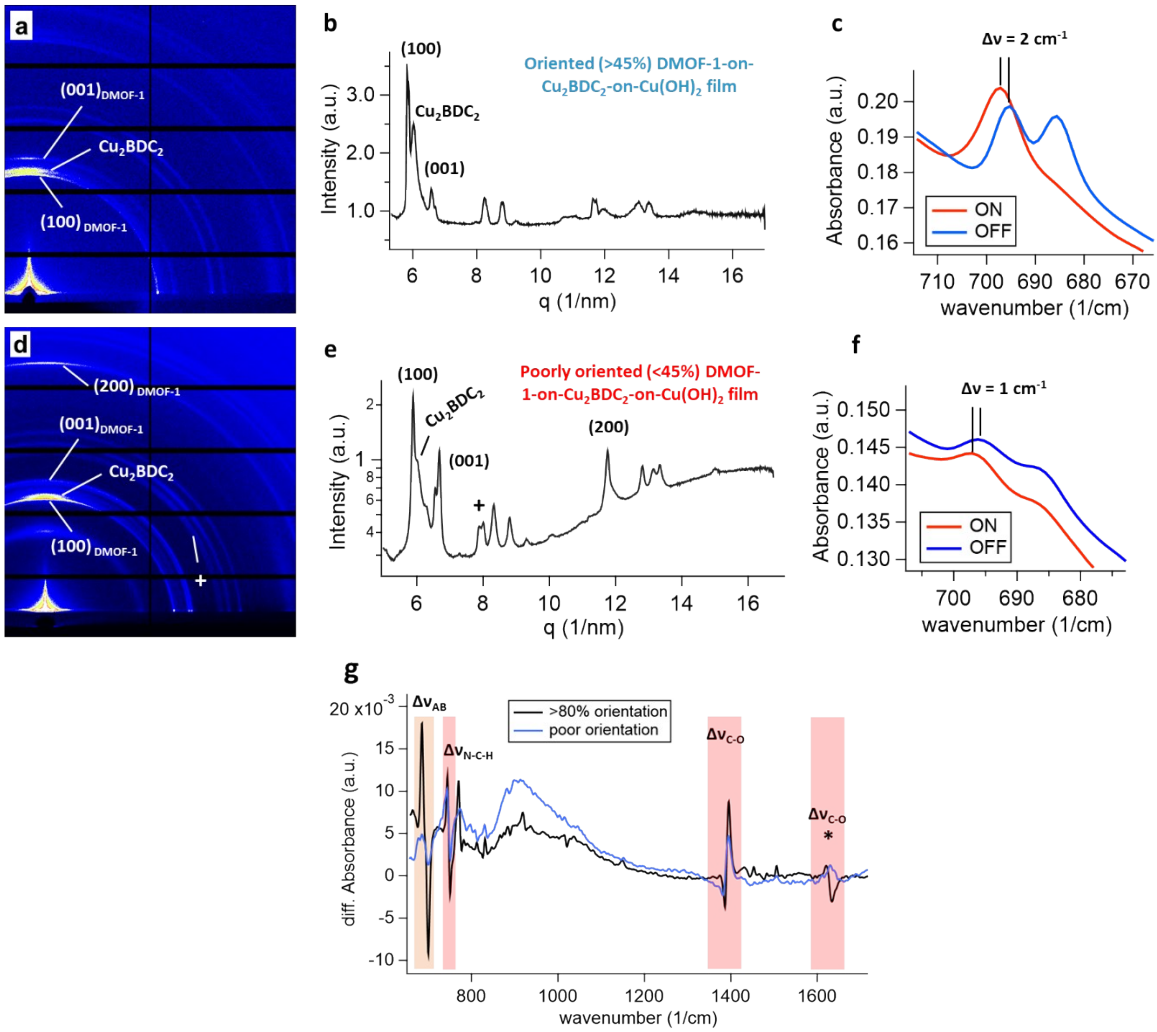

Figure S13 Influence of DMOF-1-on-Cu_2BDC_2-on-$Cu(OH)_2$ film orientation on photo-switching. a, 2D GIWAXS pattern of the oriented (>45%) **DMOF-1** film,[2] with the strong reflections arising from the (100)/(001) planes and the Cu_2BDC_2 structure indicated in the radial integrated pattern in (**b**). The azobenzene molecules in the **DMOF-1** pores isomerize between the *trans* and *cis* conformer, which consequently leads to the photo-switch of the **DMOF-1/AB** film structure (ON, OFF). **d-e**, Poorly oriented **DMOF-1** films typically show the appearance of additional strong reflections as indicated by the cross around the (110) and (101) planes. **f**, Azobenzene isomerization is only weakly pronounced indicating weak photo-switching behavior owed to the weaker interactions between the **DMOF-1** and azobenzene ($\Delta\nu_{AB}$ = 1 cm^{-1}). **g**, The shift in the C-O vibrational band between the ON and the OFF state is either entirely not present for poorly oriented films (indicated by an asterisk), or significantly weakened compared to oriented **DMOF-1/AB** films.

12. Infrared measurements for DMOF-1/AB ON/OFF photo-cycling

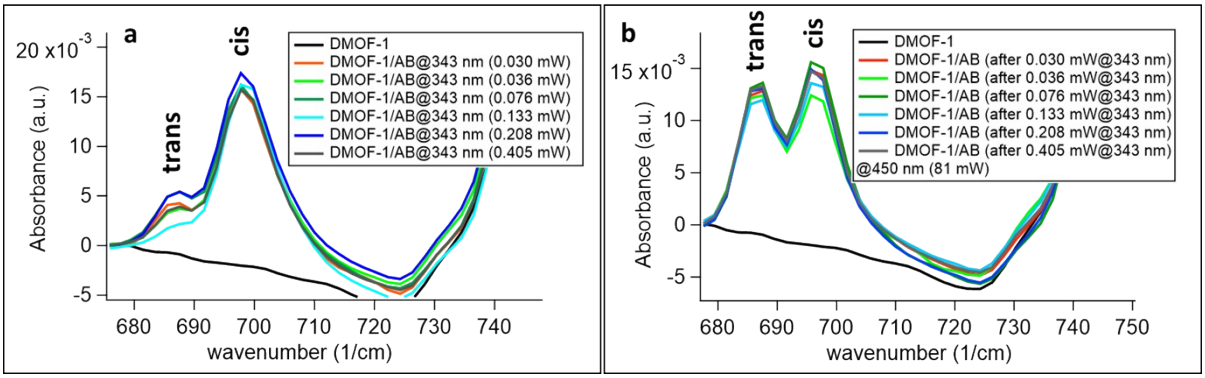

Figure S14 Infrared measurements on the ON/OFF photo-switching of DMOF-1/AB by varying the irradiation power at 343nm. a, Infrared spectra for the infiltrated azobenzene *trans* → *cis* isomerization at different UV (343 nm) irradiation powers. The pristine **DMOF-1** (black trace) lacks the two infrared bands corresponding to azobenzene. After UV excitation to the ON state, the *cis* band located at 697 cm^{-1} is strongly pronounced, whilst the *trans* band (687 cm^{-1}) shows a weak contribution and shows a decreasing contribution with increasing UV power. **b**, Back-conversion to the OFF state by LED light (450 nm, 81 mW) the *trans* azobenzene recovers to its relaxed state exhibiting an unaltered infrared intensity which is irrespective on the forward switching UV laser power used during the forward switch.

References

[1] (a) P. Falcaro, K. Okada, T. Hara, K. Ikigaki, Y. Tokudome, A. W. Thornton, A. J. Hill, T. Williams, C. Doonan, M. Takahashi, *Nature Mater* **2017**, 16, 342. (b) T. Yankova, N. Chumakova, D. Pomogailo, A. Vorobiev, *Liquid Crystals* **2013**, 40, 1135-1145.

[2] Linares-Moreau, M, Brandner, L. A., Kamencek, T., Klokic, S., Carraro, F., Okada, K., Takahashi, M., Zojer, E., Doonan, C. J., Falcaro, P., *Adv. Mat. Interfaces* **2021**, 8, 2101039.

[3] H. Amenitsch, M. Rappolt, M. Kriechbaum, H. Mio, P. Laggner, S. Bernstorff, *J. Synchrotron Rad*. **1998**, 5, 506.

[4] M. Burian, C. Meisenbichler, D. Naumenko, H. Amenitsch, SAXSDOG: open software for real-time azimuthal integration of 2D scattering images, **2020**.

[5] B. H. Toby, R. B. von Dreele, *J Appl Crystallogr* **2013**, 46, 544.

[6] D. N. Dybtsev, H. Chun, K. Kim, *Angew. Chem. Int. Ed.* **2004**, 43, 5033.

[7] a) N. Yanai, T. Uemura, M. Inoue, R. Matsuda, T. Fukushima, M. Tsujimoto, S. Isoda, S. Kitagawa, *JACS* **2012**, 134, 4501. b) Nabipour, H., Soltani, B. & Ahmadi Nasab, N. *J Inorg Organomet Polym* **2018**, 28, 1206–1213. c) M. Rödl, S. Kerschbaumer, H. Kopacka, L. Blaser, F. R. S. Purtscher, H. Huppertz, T. S. Hofer, H. A. Schwartz, *RSC Adv*. **2021**, 11, 3917.

[8] K. Okada, M. Nakanishi, K. Ikigaki, Y. Tokudome, P. Falcaro, C. J. Doonan, M. Takahashi, *Chem. Sci.* **2020**, 11, 8005.

[9] M. Burian, B. Marmiroli, A. Radeticchio, C. Morello, D. Naumenko, G. Biasiol, H. Amenitsch, *J. Synchrotron Rad*. **2020**, 27, 51.

[10] S. Lupi, A. Nucara, A. Perucchi, P. Calvani, M. Ortolani, L. Quaroni, M. Kiskinova, *J. Opt. Soc. Am. B* **2007**, 24, 959.

[11] a) D. Johannsmann, *Springer*, **2015**. b) T. Stassin, S. Rodríguez-Hermida, B. Schrode, A. Cruz, F. Carraro, D. Kravchenko, V. Creemers, I. Stassen, T. Hauffman, D. De Vos et al., *Chem. Commun*. 2019, **55**, 10056-10059.

[12] Z. Jiang, *J Appl Crystallogr* **2015**, 48, 917.

[13] L. Oesinghaus, J. Schlipf, N. Giesbrecht, L. Song, Y. Hu, T. Bein, P. Docampo, P. Müller-Buschbaum, *Adv. Mater. Interfaces* **2016**, 3, 1600403.

[14] a) K. Griffiths, N. R. Halcovitch, J. M. Griffin, *Chem. Mater*. **2020**, 32, 9925. b) J. D. Koch, J. Gronki, R. K. Hanson, *J Quant. Spectrosc. Radiat. Transf. J Quant Sprectrosc. Ra*. **2008**, 109, 2037.

[15] R. Haldar, L. Heinke, C. Wöll, *Adv. Mater*. **2020**, 32, e1905227.

[16] T. Koehler, I. Strauss, A. Mundstock, J. Caro, F. Marlow, *The Journal of Physical Chemistry Letters* **2021**, *12*, 8903-8908.

[17] Rau, H., Photoisomerization of Azobenzenes. *In Photochemistry and Photophysics, Rabek, J. D., Ed. CRC Press:* **1989**.

[18] Knoll, H., Photoisomerism of Azobenzenes. *In CRC Handbook of Organic Photochemistry and Photobiology, Horspool, W.; Lenci, F., Eds. CRC Press:* **2004**.